



Electrospun spongy zero-valent iron as excellent electro-Fenton catalyst for enhanced sulfathiazole removal by a combination of adsorption and electro-catalytic oxidation



Yi-Ping Chen^{a,b,c}, Li-Ming Yang^e, J. Paul Chen^e, Yu-Ming Zheng^{a,b,d,*}

^a CAS Key Laboratory of Urban Pollutant Conversion, Institute of Urban Environment, Chinese Academy of Sciences, 1799 Jimei Road, Xiamen 361021, China

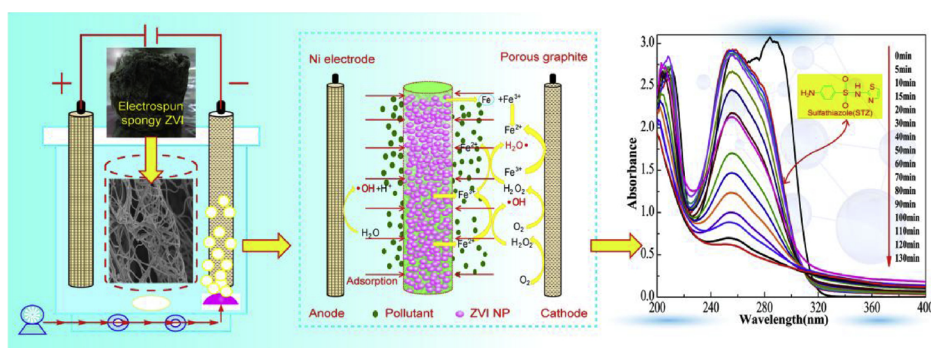
^b University of Chinese Academy of Sciences, 19A Yuquan Road, Beijing 100049, China

^c College of Resources and Environment, Quanzhou Normal University, 398 Donghai Road, Quanzhou 362000, China

^d CAS Center for Excellence in Regional Atmospheric Environment, Institute of Urban Environment, Chinese Academy of Sciences, Xiamen, Fujian 361021, China

^e Faculty of Engineering, National University of Singapore, 21 Lower Kent Ridge Road, 119077, Singapore

GRAPHICAL ABSTRACT



ARTICLE INFO

Keywords:

Adsorption
Antibiotic
Electro-catalysis
Electrospinning
Zero-valent iron

ABSTRACT

In this study, a highly active electro-Fenton catalyst, spongy zero-valent iron (ZVI), has been developed at first via in-situ synthesis of ZVI nanoparticles (NPs) on an electrospun three-dimensional (3D) nanofiber network. The spongy ZVI effectively overcame the defects of easy aggregation of ZVI NPs and ferric sludge accumulation during the electro-catalytic process. Then, a three-dimensional electro-Fenton (3D-EF) system using the as-fabricated spongy ZVI as particle catalytic electrodes was designed, which presented a significant synergistic effect of adsorption and electro-catalytic oxidation on the enhanced removal of a widely used antibiotic, sulfathiazole (STZ) from water. Adsorption experiments demonstrated that the spongy ZVI had a relative high adsorption affinity towards STZ with about 50% of the total removal within 240 min, and the adsorption equilibrium was reached in 570 min. Hydroxyl radical ($\cdot\text{OH}$) was produced in the 3D-EF system with spongy ZVI catalyst, and almost 100% STZ was removed within 5 min. Reactive oxygen species analysis verified that $\cdot\text{OH}$ was mainly responsible for the STZ degradation. Based on intermediates identified by a liquid chromatography-tandem mass spectrometry (LC-MS/MS), three pathways for the electro-Fenton oxidative degradation of STZ were proposed.

* Corresponding author at: CAS Key Laboratory of Urban Pollutant Conversion, Institute of Urban Environment, Chinese Academy of Sciences, 1799 Jimei Road, Xiamen 361021, China.

E-mail address: ymzheng@iue.ac.cn (Y.-M. Zheng).

<https://doi.org/10.1016/j.jhazmat.2019.03.043>

Received 8 October 2018; Received in revised form 24 February 2019; Accepted 9 March 2019

Available online 11 March 2019

0304-3894/ © 2019 Elsevier B.V. All rights reserved.

1. Introduction

So far, antibiotics such as sulfathiazole (STZ) have been widely used, which brought about serious threats to the ecosystem and human beings when they entered into the aqueous environment [1]. There is a growing concern over the removal of STZ and other antibiotics from water environment nowadays [2]. Several techniques have been proposed to remove the STZ, including adsorption, photocatalysis, Fenton oxidation, ion exchange, reverse osmosis, and so on [3–6]. Among them, Fenton oxidation has been regarded as a promising technology owing to its non-selective oxidation capacity by hydroxyl radical ($\cdot\text{OH}$) generated from H_2O_2 with the catalyst [7,8]. However, the practical application of homogeneous Fenton oxidation is limited by its narrow working pH range from 3 to 4, high consumption of H_2O_2 , safety risk of transportation, handling and storage of H_2O_2 , as well as the generation of ferric sludge that requires cost for disposal [9,10].

Therefore, electro-Fenton has been developed to overcome the aforementioned shortcomings. By employing an appropriate cathode, H_2O_2 could be *in-situ* generated by the electro-reduction of O_2 as shown in Eq. 1 [11]. However, the traditional two-dimensional electro-Fenton (2D-EF) system works inefficiently due to the low current density and the $\cdot\text{OH}$ cannot be fully utilized instantaneously because of its extremely short lifetime.



Recently, researchers have reported that a three-dimensional electro-Fenton (3D-EF) process significantly improved both treatment capacity and current efficiency via the introduction of particle electrodes, such as metal particles or carbon aerogel [12–14]. The particles can be easily polarized to form charged micro-electrodes by an external electric field, which shortens the distance between the pollutants and electrodes, and enhances the rate of mass transfer, leading to a higher electrolysis efficiency. In addition, in order to prevent the accumulation of ferric sludge and broaden the working pH range, heterogeneous

Fenton catalysts have been investigated. As a cost-effective and environmentally-friendly material, zero-valent iron nanoparticles (ZVI NPs) can act as the combination of adsorbent and catalyst during the electro-Fenton process [15,16]. To some extent, the synergistic effect of adsorption and catalysis plays an important role in capturing pollutants and shortening their distance which will consequently help to improve the degradation efficiency [17]. However, unfortunately, ZVI NPs are prone to aggregate on account of the weak van der Waals force, high surface energy and strong intrinsic magnetic interaction [15]. Therefore, it is difficult for ZVI NPs to uniformly disperse in water and fully interact with contaminants, which limits their widely practical applications.

In order to overcome the aforementioned problems, various supports such as activated carbon and clay were used to immobilize ZVI NPs [18–20]. Recently, electrospinning, as a highly versatile method to generate nanofibers with diameters ranging from tens to thousands of nanometers, has been used to prepare the immobilized materials. Compared with traditional supports, the morphology and diameter of electrospun nanofiber are controllable. More importantly, three-dimensional (3D) electrospun nanofiber monolith can be fabricated by selecting and modifying the nanofiber precursors. Additionally, nanofibers have the advantages of large specific surface area, small interfiber pore size, high porosity, readily accessible surface functionalization, and so on. Studies show that electrospinning is a powerful method for fabricating 3D nanofiber monoliths [21]. Furthermore, 3D electrospun nanofiber monoliths were proven to have potential applications as adsorbents and catalyst supports [21]. Due to these remarkable properties, 3D electrospun nanofiber monolith has been considered to be a promising support for constructing excellent heterogeneous catalysts.

On the other hand, polyvinyl alcohol (PVA), as an important poly-electrolyte, has attracted special attentions owing to its biodegradability, nontoxicity, water permeability and biocompatibility [22]. Some active sites such as the hydroxyl groups in PVA facilitate the adsorption of heavy metals and STZ. Mechanical strength and water-

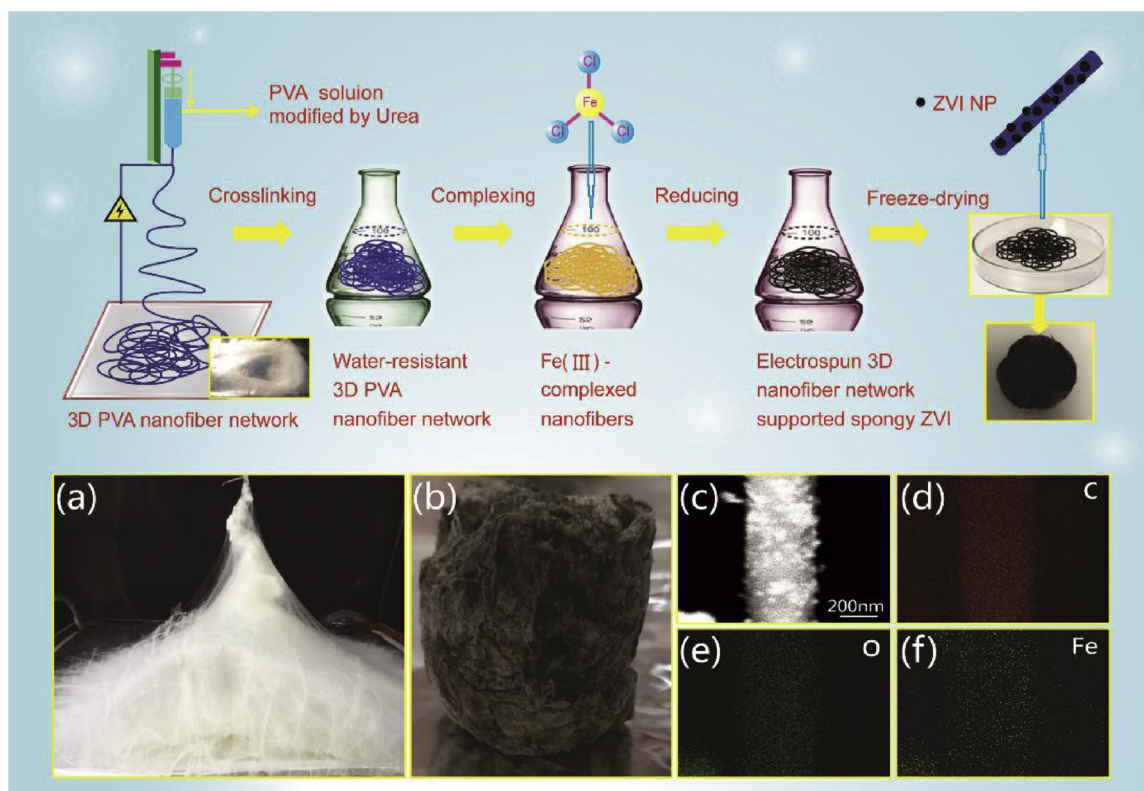


Fig. 1. Schematic illustration for the preparation of spongy ZVI: (a) 3D PVA nanofiber network; (b) immobilization of ZVI NPs on the 3D nanofiber network; (c) SEM images of nanofiber with ZVI NPs; (d–f) EDX elemental mappings of C, O and Fe, respectively.

insolubility of PVA nanofiber can be improved by cross-linking, which is helpful for avoiding collapse of the three-dimensional structure. Meanwhile, the adsorption ability can be further improved through the ion-exchange reaction, when some reactive metal ions were introduced into the cross-linking PVA structure [22].

Hence, it is expected that heterogeneous electro-Fenton process can be performed by ZVI NPs immobilization on the highly puffy 3D PVA nanofiber network, which enables a better contact between catalyst and STZ in the solution similar to the homogeneous electro-Fenton reaction. When the ZVI NPs particle electrodes are evenly packed into a reactor, a 3D-EF system will be constructed. To my knowledge, there is no attention has been paid to the usage of 3D electrospun nanofiber network as support for the fabrication of heterogeneous zero-valent iron-based catalysts to be applied in a 3D-EF system.

This work aims to fabricate a highly efficient heterogeneous electro-Fenton catalyst with ZVI NPs as the active species, which are supported by a 3D PVA nanofiber network. The developed electrospun 3D nanofiber network supporting catalyst is known as spongy ZVI. On this basis, a 3D-EF system using the spongy ZVI as the catalytic particle electrodes is constructed. The performance of the combination of adsorption and electro-catalysis removal of STZ under different conditions is systematically evaluated in detail. Finally, the catalytic degradation mechanism of STZ is proposed.

2. Materials and methods

2.1. Reagents

The reagents used were presented in Supplementary Data, Text S1.

2.2. Preparation of electrospun spongy zero-valent iron

2.2.1. Fabrication of water-resistant electrospun 3D PVA nanofiber network

Ten grams of PVA powder was firstly dissolved into 100 mL water at 80 °C under magnetic stirring to prepare the PVA solution. Then, 20% urea was added to the PVA solution, and the mixture was stirred at 30 °C for 3 h to get a viscoelastic solution. Subsequently, the PVA/urea solutions were then moved into a plastic syringe with a metallic needle, which was coupled with a voltage of 26 kV. A flat aluminum foil was used as the nanofiber collector, which was connected to a negative voltage of -6 kV. The distance between the spinneret and the collector was kept at 15 cm. The feeding rate of the PVA solution was controlled

at 2.5 mL h⁻¹ using a Veryark TCI-IV syringe pump (Guangxi, China), while the humidity and temperature were maintained at 50 ± 5% and 25 °C, respectively. A 3D PVA nanofiber network was constructed on the collector, which was further crosslinked in ethanol solution containing 0.15 M glutaraldehyde and 0.05 M HCl to form water-resistant 3D PVA nanofiber network. Finally, the 3D PVA nanofiber network was rinsed by deionized water to remove the residue solvent.

2.2.2. Synthesis of electrospun 3D nanofiber network supporting spongy ZVI

The synthetic procedure of the electrospun 3D PVA nanofiber network supporting spongy ZVI was shown in Fig. 1. In brief, the water-resistant 3D PVA nanofiber network was immersed into a 0.4 M FeCl₃ aqueous solution under continuously stirring for 3 h to allow Fe³⁺ to complex with the hydroxyl groups of PVA and the unreacted aldehyde groups generated during the crosslinking process, and then rinsed with deionized water. Meanwhile, ZVI NPs were in-situ synthesized and immobilized by reducing the Fe(III) ions complexed with nanofibers using NaBH₄ solution (20 mM, 200 mL) [23]. The obtained black 3D nanofiber network with immobilized ZVI NPs was washed with deionized water and then frozen for more than 2 h. After that, the 3D nanofiber network with immobilized ZVI NPs was vacuum-freeze dried for 2 days to form the spongy ZVI, which was stored in a desiccator for further experiments.

2.3. Characterization of the spongy ZVI

Characterization of the spongy ZVI was described in Supporting information, Text S2.

2.4. Adsorption experiments

Adsorption kinetics experiments were performed to assess the adsorption performance of spongy ZVI in a shaker with a rate of 120 rpm. In the adsorption experiments, no additional compressed air flow was introduced into and no electric current was applied. The spongy ZVI, weighing 100 mg, was added into 100 mL of 50 mg L⁻¹ STZ solution at pH 5. Aliquot of 1.5 mL of solution was taken at given time and immediately filtered with a 0.45 μm membrane filter prior to the UV-vis spectrometer (Puxi TU-1810, Beijing) measurement at the wavelength of 283 nm.

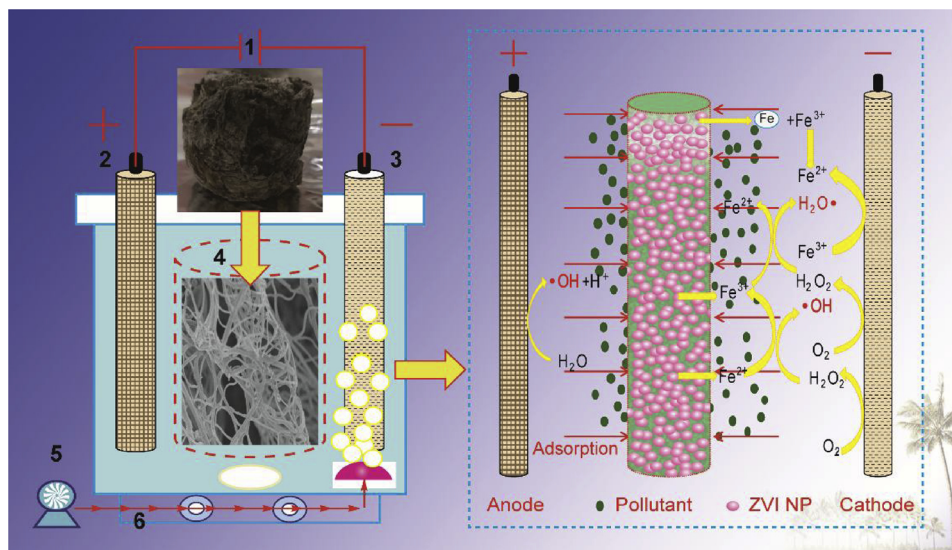


Fig. 2. Schematic illustration of the 3D-EF system.

1. D.C power supply; 2. Ni electrode; 3. Porous graphite electrode; 4. Electrospun spongy ZVI; 5. Air pump; 6. Magnetic agitator.

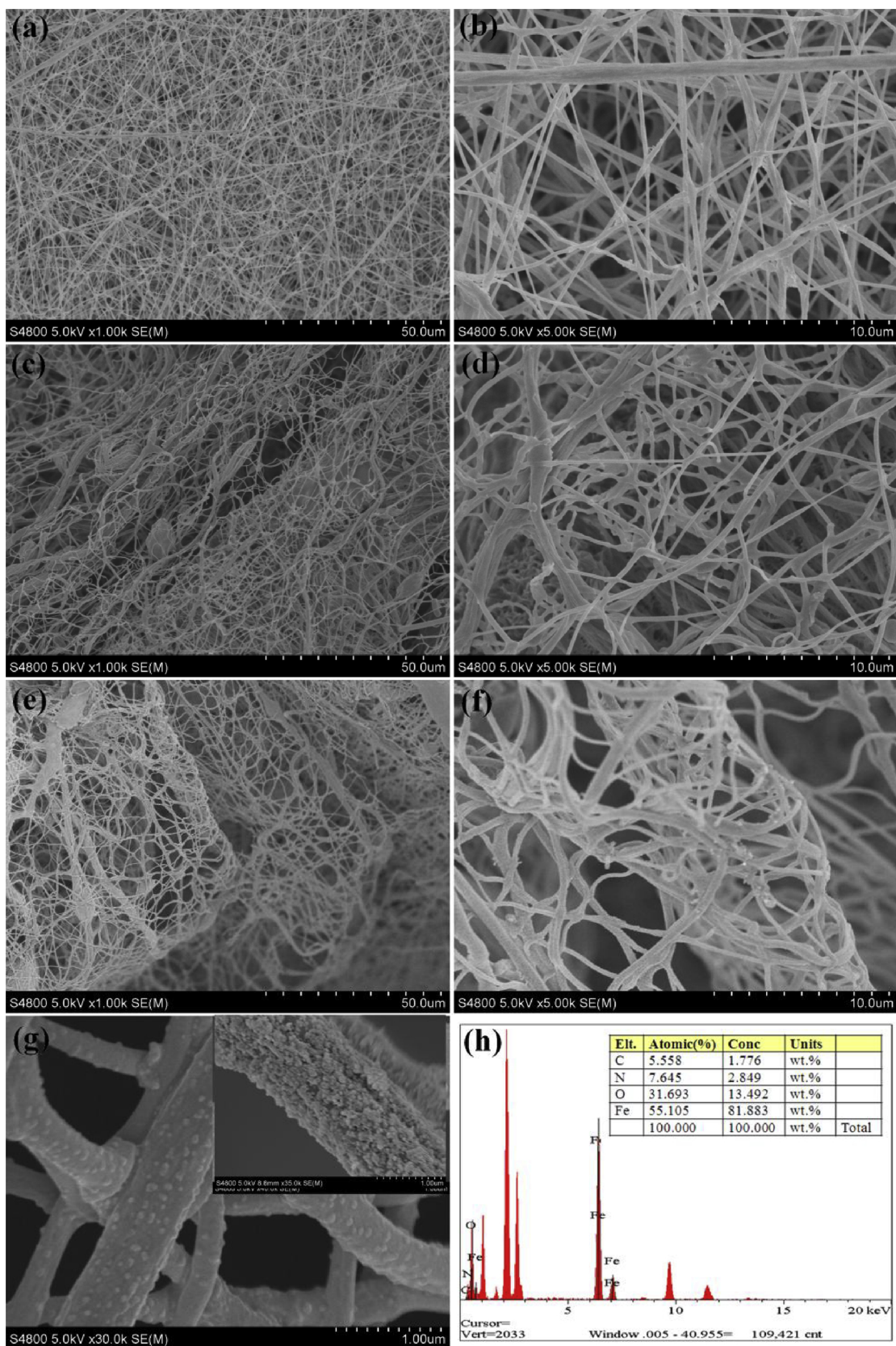


Fig. 3. SEM images of the 3D electrospun nanofibers: (a) 3D PVA nanofiber network (with low magnification of 1.0k ×); (b) 3D PVA nanofiber network (with high magnification of 5.0k ×); (c) water-resistant 3D network (with low magnification of 1.0k ×); (d) water-resistant 3D network (with high magnification of 5.0k ×); (e) sponge ZVI (with low magnification of 1.0k ×); (f) sponge ZVI (with high magnification of 5.0k ×); (g) sponge ZVI (with high magnification of 30.0k ×); and (h) EDX graph of sponge ZVI.

2.5. 3D-E-Fenton experiments

The coupled adsorption and electro-catalytic oxidation removal performance of the STZ were tested in a 3D-EF system with a galvanostatic mode controlled by a DC power supply (KXN-3040D, Shenzhen) (Fig. 2). Briefly, a 10 cm × 4 cm porous graphite cathode and a Ni anode with the same dimension were aligned parallel to each other at a distance of 5 cm while the spongy ZVI was placed between them in the 3D-EF reactor without direct electric contact. 400 mL STZ solution (50 mg L⁻¹) was added into the 3D-EF reactor with 50 mM Na₂SO₄ as the supporting electrolyte. An air flow of 1.5 L min⁻¹ was continuously injected into the solution through a disk-shaped porous aerator (60 mm in diameter and 15 mm in thickness) placed under the cathode. The experiments were carried out at around 15 °C. The catholyte was pre-saturated with compressed air for 30 min before each experiment. Meanwhile, magnetic stirring was maintained to enhance the mass transfer rate of the pollutants towards/from the electrodes. The evolution of UV spectrum from 200 to 350 nm was recorded at a certain time interval. In the recycle tests, the spongy ZVI used was soaked in a 1.0 M NaBH₄ solution for 5 min, followed by washing with deionized water and vacuum-freeze drying. The other experimental conditions were kept the same with the subsequent runs.

2.6. Chemical analysis

The detailed chemical analysis is provided in Supporting Information, Text S3.

3. Results and discussion

3.1. Preparation and characterization of the spongy ZVI

As shown in Fig. 1a, the PVA nanofibers presented a loose three-dimensional fibrous morphology, which might be due to the following reasons: (a) The addition of urea increased the electrical conductivity and decreased the viscosity of the PVA solution, thereby improving the electro-spinnability of the blend solution [24]; (b) Owing to the significant increase of electrostatic force, the rapidly produced electrospun nanofibers were randomly deposited to form a three-dimensional structure; (c) The repulsion force between the electrospun nanofibers caused by the charge accumulation led to a fluffy structure.

After ZVI NPs immobilization, the color of electrospun 3D PVA nanofiber network turned into black, and the structure became more compact (Fig. 1b). It was observed that a great many ZVI NPs were evidently distributed on the surface of 3D PVA nanofiber network to form spongy ZVI (Fig. 1c). The energy-dispersive X-ray analysis (EDX) elemental mappings (Fig. 1d–f) confirmed that the heterogeneous spongy ZVI was made up of C, O and Fe elements. The C and O elements were derived from the electrospun 3D PVA nanofiber skeleton, and the Fe element came from the ZVI NPs coating on the surface of fibers.

As shown in Fig. 3, scanning electron microscopy (SEM) micrographs further revealed the morphology of as-electrospun 3D nanofibers. These 3D PVA nanofibers had a loose porous reticular structure (Fig. 3a). The partial zoom-in image (Fig. 3b) showed that the PVA nanofibers had a smooth surface with an average diameter around 270 nm. After cross-linking, a small part of the nanofibers, originally straight, merged and entangled with each other due to the intersections/fuses of the 3D nanofiber network. The mechanical strength and stability of the water-resistant 3D nanofiber network were improved, and the morphology and structure of the nanofiber network were retained (Fig. 3c & d).

However, the smooth PVA nanofibers became rough and the average diameter of the nanofibers on sponge ZVI was 300 nm after the immobilization of ZVI NPs, which were uniformly dispersed in the 3D nanofiber network (Fig. 3e–g). Such a geometry efficiently improved the interfacial contact area of nanofiber network and suppressed the

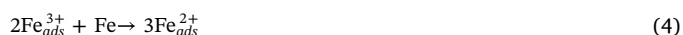
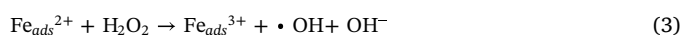
agglomeration of ZVI NPs. In addition, the structure of the 3D nanofiber network became more loose and porous, indicating the well coexistence of the zero-valent iron phase and the carbon phase. Therefore, as a support, the water-resistant 3D nanofiber network increased the stability of the ZVI NPs. The inset in Fig. 3g showed that the shape of ZVI NPs was granular, which significantly increased the specific surface area of the PVA nanofibers. The EDX analysis (Fig. 3h) confirmed that ZVI NPs has been successfully immobilized in the 3D nanofiber network.

The results of X-ray diffraction (XRD), Fourier transform infrared spectrometer (FTIR) and Brunauer-Emmett-Teller (BET) analysis were described in detail in Text S4–S6 (Supplementary Information), respectively, which further proved the successful integration of uniform and monodisperse ZVI NPs into the 3D PVA nanofiber networks, and the spongy ZVI showed a relatively high specific surface area.

3.2. Performance of the 3D-EF system for STZ removal

As depicted in Fig. 2, the STZ in the 3D-EF system is anticipated to be removed in two ways: adsorption and catalytic oxidation. On one hand, due to the large specific surface area and high porosity of spongy ZVI, its adsorption towards STZ is inevitable, which to capture STZ and increases the concentration of STZ on the spongy ZVI. On the other hand, since the spongy ZVI is rich in catalytic active sites for Fenton reaction, it can be foreseen that the decomposition of H₂O₂ will be a surface catalytic enhanced process. At first, the active O₂ is in-situ reduced to H₂O₂ via a two-electron reduction on the interface between the spongy ZVI and the bulk solution phase. Meanwhile, under weak acidic conditions, some iron nanoparticles on the surface of the 3D nanofiber network may in-situ produce Fe²⁺ (Eq. 2). Next, the generated H₂O₂ molecules are catalytically decomposed into ·OH, and the Fe²⁺ ions are oxidized into Fe³⁺ promptly (Eq. 3). Then, the generated ·OH quickly reacts with the STZ molecules concentrated by the spongy ZVI, which are degraded into intermediates or completely mineralized.

According to Eq. 4, the conversion of Fe³⁺ into Fe²⁺ takes place at the metal surface, which facilitates the recycling of Fe [16]. Hence, the 3D-EF system avoids continuously dissolving iron species into the solution, which is often faced by the homogeneous Fenton process [25]. Moreover, during the electrochemical reaction, the ZVI NPs on the spongy ZVI can produce charged microelectrodes that are conducive to improving the degradation efficiency of STZ due to the polarization of external electric field.



As discussed above the mineralization of STZ and the regeneration of Fe occur simultaneously in the 3D-EF system. Furthermore, adsorption and oxidation facilitate each other, greatly promoting the STZ removal. Additionally, during the electro-Fenton process, the spongy ZVI as a heterogeneous electro-Fenton catalyst overcomes the disadvantage of the generation and accumulation of iron sludge.

3.2.1. Adsorption performance of the spongy ZVI

To assess the adsorption performance of the spongy ZVI for STZ removal and facilitate the enrichment of STZ around the spongy ZVI particle electrodes in the 3D-EF system, adsorption kinetics experiments are conducted, and the result is illustrated in Fig. 4a. It is clearly shown that the amount of STZ adsorbed on the spongy ZVI increases with time, and the adsorption equilibrium is obtained within 570 min. The STZ adsorption is relatively fast and about 50% of the total adsorption is finished in 240 min. This may be due to the fact that initial active sites on the surface of spongy ZVI are vacant and the STZ concentration gradient is high as well. After about 570 min, all the adsorption sites are

filled with STZ, resulting in an unchanged adsorption percentage.

Three commonly used kinetics models, named pseudo-first-order, pseudo-second-order and Weber-Morris models [26,27], are proposed to interpret the experimental kinetic data, as shown in Fig. 4b–d, respectively. The results show that the adsorption kinetics fits well with the pseudo-second-order model, and the whole adsorption behavior can be divided into two different phases: external diffusion and intra-particle diffusion. Obviously, intra-particle diffusion is the dominant controlling step for STZ adsorption on the spongy ZVI. Details are described in Supporting Information, Text S7.

This superior adsorption performance of spongy ZVI towards STZ could be ascribed not only to high specific surface, but also to its abundant adsorption active sites, e.g. oxygen-containing functional groups and Fe species. FTIR analysis (Text S5) confirmed that the spongy ZVI involved abundant oxygen-containing functional groups and Fe species, both of which were beneficial to the STZ adsorption [28]. In addition, the binding effect of hydrogen bonds and the electrostatic attraction (Text S8) between the spongy ZVI and the STZ molecules could also lead to a good adsorption performance [29].

3.2.2. Coupled adsorption and electro-catalytic oxidation performance of the spongy ZVI

To study the synergistic effect of adsorption and electro-catalytic oxidation of spongy ZVI in the 3D-EF system, UV–vis spectra analysis about STZ solution are periodically conducted during the electro-Fenton process (Fig. 5). The absorption spectrum of STZ solution mainly consists of three bands at the wavelengths of 217, 254 and 283 nm, which are corresponding to substituted sulfonyl group, benzene

structure and thiazole ring, respectively. The latter is taken as a reference for the determination of the STZ concentration using a UV–vis spectrophotometer.

As shown in Fig. 5a–c, all the peak intensities of the STZ solution decreased gradually in the different electro-Fenton systems, indicating the removal of STZ. Based on the absorption peak at 283 nm, it was found that both the two 3D-EF systems with ZVI NPs or spongy ZVI as the catalyst could almost completely remove STZ within 5 min. The fast disappearance of the absorption peak at 283 nm could be correlated with the decomposition of thiazole ring of the STZ. The STZ removal rate of these two 3D-EF systems was two times higher than that of the electro-Fenton system without a catalyst. A comparison of the STZ removal efficiency between the spongy ZVI and other catalysts reported in previous literatures was summarized in Table S1, which revealed that the STZ removal efficiency of spongy ZVI was higher than that of other catalysts [30–34].

On the contrary, the absorption peak at 254 nm remarkably increased within 5 min in both the two 3D-EF systems with catalysts (insets in Fig. 5b & c), indicating that some intermediate products containing benzene ring were formed during the rapid destruction of the STZ structure. Based on the UV spectrum, the liquid chromatography-tandem mass spectrometry (LC–MS/MS) analysis also proved that some compounds such as aniline were produced during the electro-Fenton removal of STZ, which might be more difficult to be oxidized than the thiazole ring. After 5 min, the intensity of the absorption band at 254 nm gradually decreased, indicating the degradation rate of benzene ring was much slower and the thiazole ring was more susceptible to the oxidation process. Meanwhile, the absorption band at

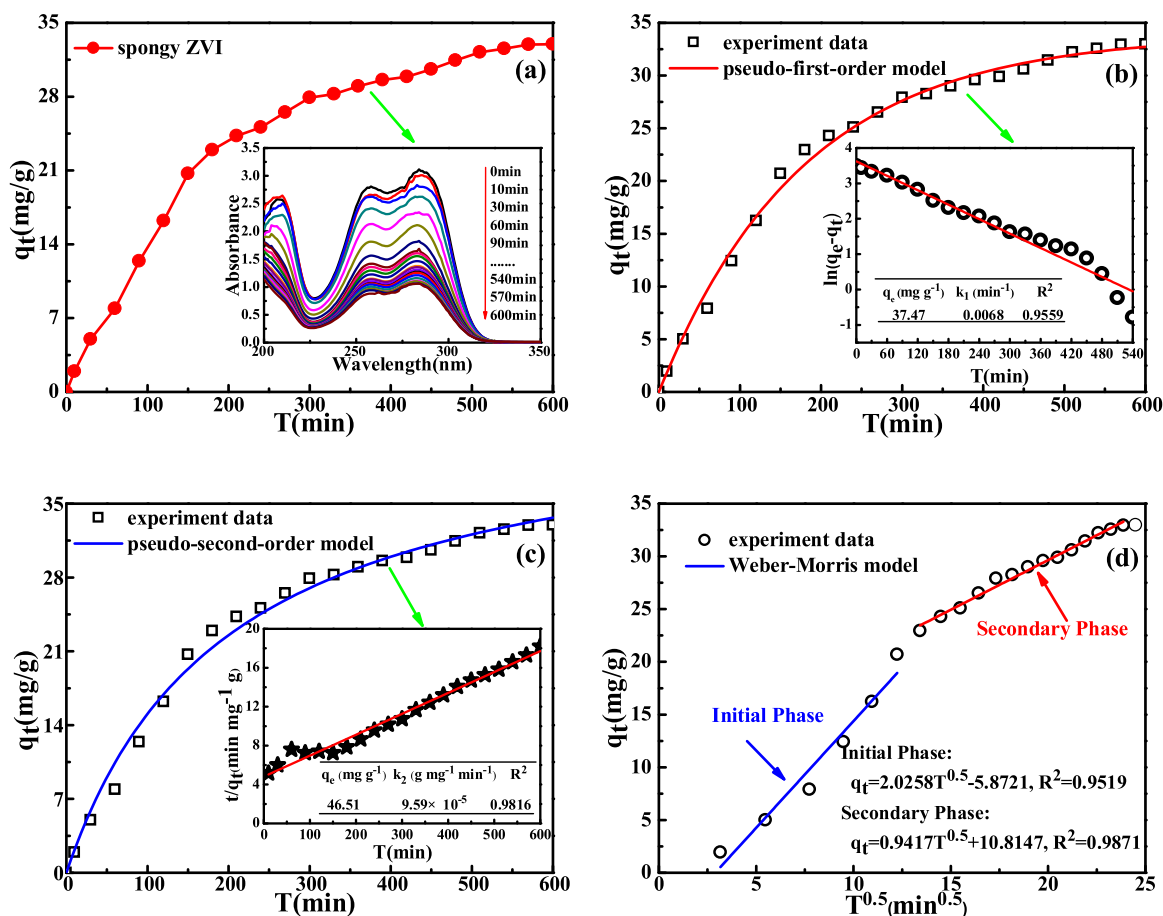


Fig. 4. (a) Adsorption kinetics of STZ on the spongy ZVI. The inset is UV–vis spectra of STZ solution during the adsorption process by the spongy ZVI. (b) Pseudo-first-order model, (c) Pseudo-second-order model and (d) Weber-Morris model for STZ adsorption on spongy ZVI. Experimental conditions: [adsorbent] = 1 g L⁻¹; [STZ] = 50 mg L⁻¹; pH = 5.

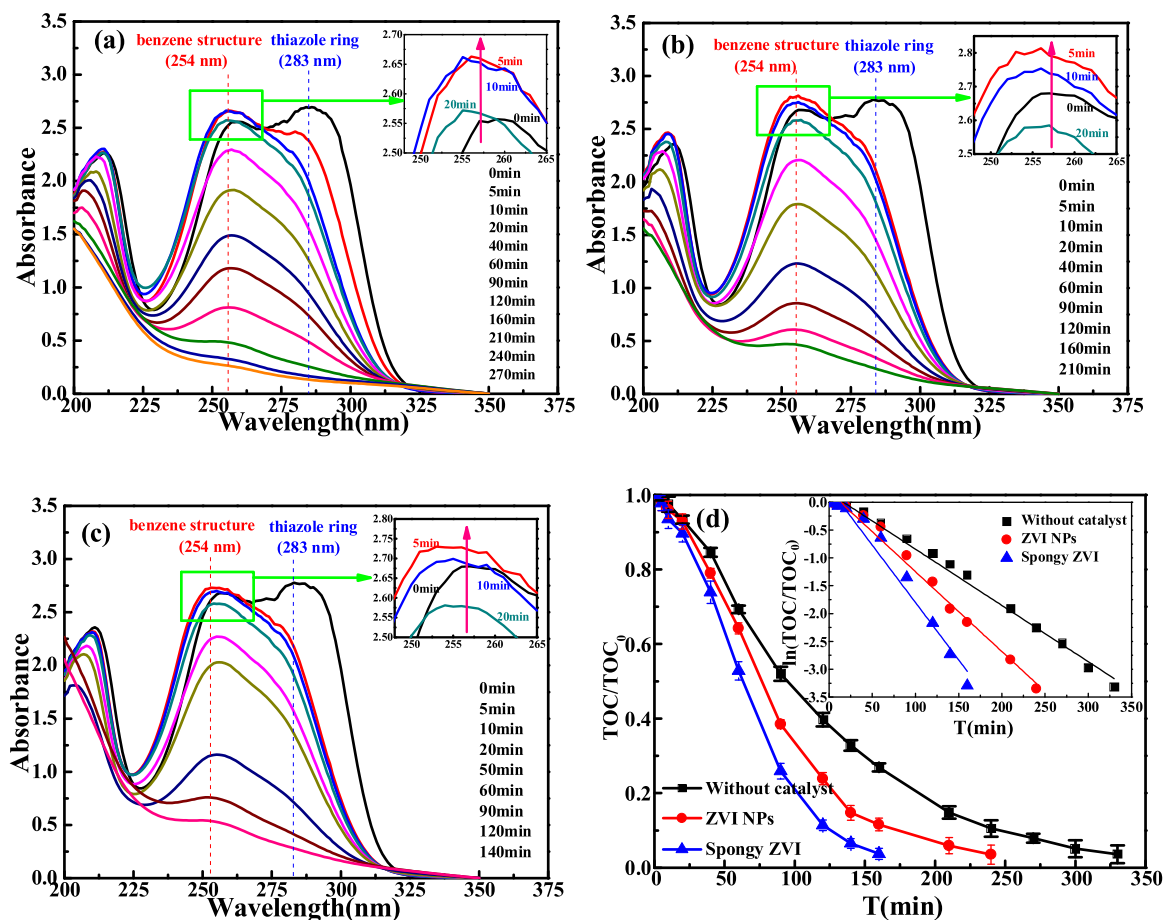


Fig. 5. Extinction spectra of the STZ solution at different time during the electro-Fenton process: (a) without catalyst, (b) [ZVI NPs] = 1 g L⁻¹ (c) [spongy ZVI] = 1 g L⁻¹; (d) TOC variation of the STZ solution with reaction time in the different electro-Fenton systems, and the inset shows the plots of ln(TOC/TOC₀) versus reaction time. Experimental conditions: $j = 7.5 \text{ mA cm}^{-2}$; pH = 5; [Na₂SO₄] = 50 mM; [STZ] = 50 mg L⁻¹.

217 nm also diminished steadily, indicating that both the sulfonyl and benzene structures were oxidized and further transformed to small molecules by the $\cdot\text{OH}$ [35].

In order to investigate the mineralization of the STZ, the total organic carbon (TOC) variations of the STZ solution in the three electro-Fenton systems were measured and demonstrated in Fig. 5d. It was clear that the TOC reduction of the STZ solution in the 3D-EF system with spongy ZVI showed much faster than that in the electro-Fenton systems without a catalyst or with ZVI NPs as the catalyst. After 140 min of reaction time, the TOC was reduced by 93.5%, 85.3% and 62.7% in the electro-Fenton systems with the spongy ZVI catalyst, ZVI NPs catalyst, and without a catalyst, respectively. As presented in the inset of Fig. 5d, the kinetics of TOC removal in all the systems approximately followed the pseudo-first-order law, and the corresponding rate constants were 0.0205, 0.0144 and 0.0101 min⁻¹, respectively. Furthermore, it should be noted that the Fe content in the spongy ZVI was only 30%. Therefore, compared with the ZVI NPs, the heterogeneous electro-Fenton system with spongy ZVI as the catalyst exhibited higher activity.

Additionally, the effect of the initial pH value on the removal efficiency of STZ as well as the stability and reusability of the spongy ZVI in the 3D-EF system were further evaluated. The results are described in detail in the Supporting Information, Text S9-S10. Compared with homogeneous catalysts, the spongy ZVI also exhibited remarkable pH-tolerant performance, excellent sustained catalytic activity and recycling capability.

The rapid removal of STZ in the 3D-EF system might be ascribed to the synergistic effect between adsorption and electro-catalytic

oxidation of the spongy ZVI. On one hand, the enrichment of STZ around the catalytic active center of the ZVI NPs caused by the adsorption of spongy ZVI was conducive to improve the electro-catalytic oxidation efficiency of the trace STZ in the aqueous solution. Hu et al. and Zhang et al. have reported the similar phenomenon [25,36]. Besides, the spongy ZVI enabled a better contact between the $\cdot\text{OH}$ and the STZ in water due to its curly and loose three-dimensional fibrous morphology. On the other hand, the electro-catalytic oxidation of STZ could promote the adsorption of STZ on the spongy ZVI. According to the above analysis and calculation, the removal rate of STZ by the combination of electro-catalytic oxidation and adsorption was 0.0205 min⁻¹, which was relatively higher than that (0.0068 min⁻¹) by adsorption only. Therefore, it could be predicted that the STZ was rapidly oxidized by the generated active species such as $\cdot\text{OH}$, when it was adsorbed onto the spongy ZVI. Meanwhile, the adsorptive active sites were regenerated due to the catalytic oxidation of the adsorbed STZ, which promoted the adsorption process. In addition, compared with 2D electrodes, the conductivity and the mass transfer were also improved by the spongy ZVI [13].

In the 3D-EF system, a series of catalytic oxidation reactions might occur on the spongy ZVI surface (heterogeneous reaction) and in aqueous solution (homogeneous reaction). In order to confirm the participation of Fe species in the surface electro-Fenton catalytic reaction, the X-ray photoelectron spectra (XPS) analyses of the spongy ZVI in the 3D-EF system before and after the STZ removal were carried out as seen in Text S11 of Supporting Information. It could be concluded that the ZVI NPs fixed in the 3D nanofiber network had a core-shell-like structure, which contained a main core of ZVI (Fe⁰) and a shell of other Fe

species (Fe(II), Fe(III)). In the aqueous solution, the concentrations of Fe leached from the spongy ZVI in the 3D-EF system were monitored, and the results were presented in Fig. 6a. As the reaction progress, the concentration of dissolved iron species, especially Fe^{2+} , increased to a certain level and then decreased. This means that the homogenous Fenton reaction might occur in the bulk solution [37,38]. The mineralization of STZ was the result of a combination of heterogeneous and homogeneous catalytic processes. However, due to the low concentration of dissolved iron, the heterogeneous Fenton oxidation played a more important role in the STZ degradation.

The amount of H_2O_2 produced from oxygen reduction at cathode is crucial in an electro-Fenton process. Hence, it is necessary to investigate the amount of H_2O_2 generated in the 3D-EF system with different catalysts. According to Fig. 6a, in the electrolysis system without any catalyst, the accumulated concentration of H_2O_2 increases with the increment of reaction time, and achieves a value of 140 mg L^{-1} after 150 min electrolysis. After that, the accumulated concentration of H_2O_2 gradually reached a steady state. This behavior can be explained by assuming that H_2O_2 is electronically generated and simultaneously destroyed in the anode at the same rate [39]:



However, using ZVI NPs or spongy ZVI as catalysts in the 3D-EF system, the accumulated concentration of H_2O_2 is much lower than without any catalyst in the electrolysis system, which only reached a steady value of about 70 mg L^{-1} and 30 mg L^{-1} after 150 min electrolysis (Fig. 6a), respectively. This fact indicates that the ZVI NPs and the spongy ZVI can act as heterogeneous catalysts to decompose the H_2O_2 generated by the cathode to activate the Fenton reaction. In 3D-EF system with the spongy ZVI as a catalyst, H_2O_2 decomposes faster than those of the other two systems, which can be attributed to the better catalytic performance of the spongy ZVI towards the reactions as shown in Eqs. 2–4 and 7 [39,40].



To further confirm the involved mechanism, the benzoic acid is employed as a probe reagent to verify the generated $\cdot\text{OH}$ after 90 min, 180 min and 270 min electrolysis in the three different electro-Fenton systems. As shown in Fig. 6b, more $\cdot\text{OH}$ was generated in the heterogeneous electro-Fenton system using spongy ZVI as the catalyst, which well agrees with the analysis of H_2O_2 . This also suggests that $\cdot\text{OH}$ was

the dominant oxidative specie in the electro-Fenton system.

3.3. Degradation pathways of STZ in the 3D-EF system

To gain insight into the degradation mechanism of STZ in the electro-Fenton process, the intermediates were analyzed by LC-MS/MS. Based on the total ion chromatogram (TIC) and the corresponding retention time (t_R) of peaks, total 9 main intermediates were identified (correspondingly labeled TP-1 to TP-9, as shown in Fig. S9).

According to molecular structures of the detected intermediates, three possible STZ degradation pathways in the 3D-EF system were proposed (Fig. 7). Pathway A involves the hydroxylation of phenyl ring, leading to the formation of (OH)STZ (TP-1) or (OH)₂STZ (TP-2). Then, the $\cdot\text{OH}$ attacks at the S–N bond in TP-1 or TP-2 to produce (OH)sulfanilic acid (TP-8) or (OH)₂sulfanilic acid (TP-9) and 2-aminothiazole (TP-3), respectively. Pathway B is initiated by the oxidative degradation of the S–N bond in STZ by $\cdot\text{OH}$ to generate 2-aminothiazole (TP-3) and sulfanilic acid (TP-4), which is further oxidized to form aniline (TP-7). Pathway C begins with the hydroxylation of thiazole ring, resulting in the formation of TP-5. Subsequently, TP-6 is produced by the further oxidation of TP-5, corresponding to the breakdown of its thiazole ring. Additionally, the $\cdot\text{OH}$ attacks at C–S bond in TP-6 to produce TP-7. Finally, the intermediates may be further converted to smaller molecule, or even partially mineralized, which is proven by the TOC analysis. Combined with the UV-vis spectra of the STZ solution, the thiazole ring of STZ is rapidly decomposed in a short time, which means that the pathway C may be the main degradation process during the degradation of STZ.

4. Conclusions

In summary, a facile synthetic strategy was developed for fabricating spongy ZVI based on electrospun 3D nanofiber networks. The spongy ZVI presented a relative high adsorption affinity to STZ, due to its loose structure and high content of ZVI NPs. Taking advantage of the spongy ZVI as particle catalytic electrodes, a 3D-EF system was designed to achieve almost 100% STZ removal within 5 min by a combination of adsorption and electro-catalytic oxidation. The $\cdot\text{OH}$ generated in the 3D-EF system played an important role in the STZ removal. According to the intermediates identified, three possible pathways for the STZ degradation were proposed. This work suggests that the 3D-EF system has great potential in the removal of antibiotics from water.

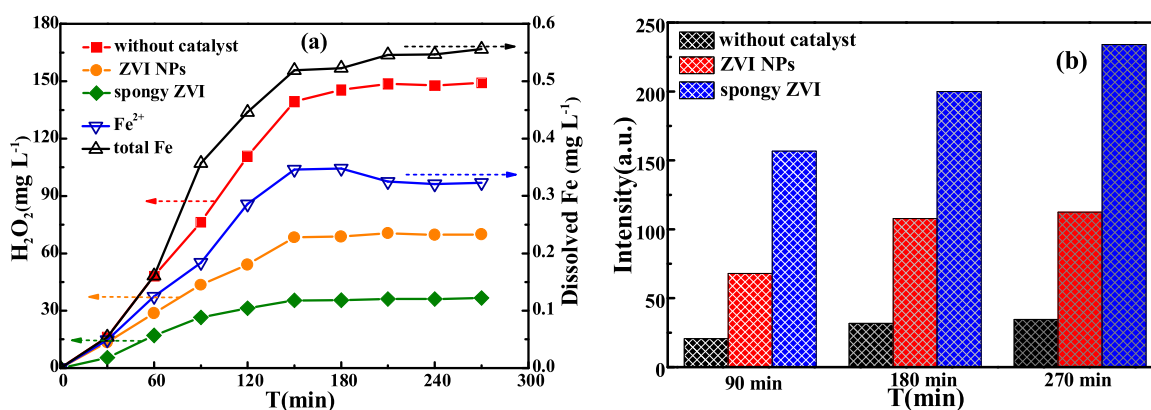


Fig. 6. The concentration variation of (a) H_2O_2 in the electro-Fenton systems without any catalyst, with 1 g L^{-1} ZVI NPs catalyst and with 1 g L^{-1} spongy ZVI, respectively and the concentration of dissolved iron species in the electro-Fenton systems with 1 g L^{-1} spongy ZVI; (b) $\cdot\text{OH}$ with reaction time in the electro-Fenton systems without any catalyst, with 1 g L^{-1} ZVI NPs catalyst and with 1 g L^{-1} spongy ZVI, respectively. Experimental conditions: $[\text{Na}_2\text{SO}_4] = 50 \text{ mM}$, $j = 7.5 \text{ mA cm}^{-2}$, $\text{pH} = 5$.

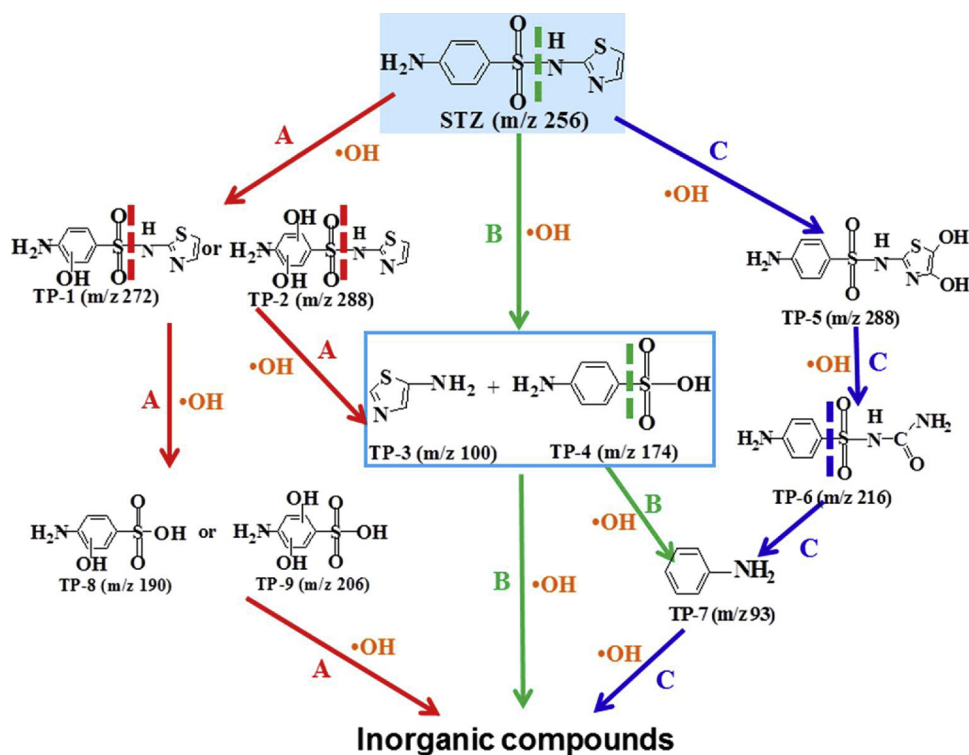


Fig. 7. Proposed degradation pathways of STZ in the 3D-EF process.

Acknowledgements

This work was supported by the National Natural Science Foundation of China (Grant Nos. 5153000136 and 51578525), and the Natural Science Foundation of Fujian Province, China (Grant No. 2017J01713).

Appendix A. Supplementary data

Supplementary material related to this article can be found, in the online version, at doi:<https://doi.org/10.1016/j.jhazmat.2019.03.043>.

References

- M.B. Feng, Z.Y. Wang, D.D. Dionysiou, V.K. Sharma, Metal-mediated oxidation of fluoroquinolone antibiotics in water: a review on kinetics, transformation products, and toxicity assessment, *J. Hazard. Mater.* 344 (2018) 1136–1154.
- L.H. Santos, A.N. Araújo, A. Fachini, A. Pena, C. Delerue-Matos, M. Montenegro, Ecotoxicological aspects related to the presence of pharmaceuticals in the aquatic environment, *J. Hazard. Mater.* 175 (2010) 45–95.
- C. Sophia, E.C. Lima, Removal of emerging contaminants from the environment by adsorption, *Ecotoxicol. Environ. Saf.* 150 (2018) 1–17.
- Z. Hu, Z. Shen, J.C.M. Yu, Converting carbohydrates to carbon-based photocatalysts for environmental treatment, *Environ. Sci. Technol.* 51 (2017) 7076–7083.
- C. Feng, C. Tsai, C. Ma, C. Yu, C. Hou, Integrating cost-effective microbial fuel cells and energy-efficient capacitive deionization for advanced domestic wastewater treatment, *Chem. Eng. J.* 330 (2017) 1–10.
- J.Y. Choi, H.S. Lee, Y. Choi, S. Kim, S. Lee, S. Lee, W.Y. Choi, J. Lee, Heterogeneous photocatalytic treatment of pharmaceutical micropollutants: effects of wastewater effluent matrix and catalyst modifications, *Appl. Catal. B-Environ.* 147 (2014) 8–16.
- A. Aboudalle, H. Djelal, F. Fourcade, L. Domergue, A.A. Assadi, T. Lendormi, S. Taha, A. Amrane, Metronidazole removal by means of a combined system coupling an electro-Fenton process and a conventional biological treatment: by-products monitoring and performance enhancement, *J. Hazard. Mater.* 359 (2018) 85–95.
- X. Li, Y. Cui, Y. Feng, Z. Xie, J. Gu, Reaction pathways and mechanisms of the electrochemical degradation of phenol on different electrodes, *Water Res.* 39 (2005) 1972–1981.
- L. Clarizia, D. Russo, I.D. Somma, R. Marotta, R. Andreozzi, Homogeneous photo-Fenton processes at near neutral pH: a review, *Appl. Catal. B-Environ.* 209 (2017) 358–371.
- C. Chun, Z. Zhang, J. Liu, N. Shan, H. Zhang, D.D. Dionysiou, Visible light-assisted heterogeneous Fenton with $ZnFe_2O_4$ for the degradation of Orange II in water, *Appl. Catal. B-Environ.* 182 (2016) 456–468.
- Z.M. Qiang, J. Chang, C. Huang, Electrochemical regeneration of Fe^{2+} in Fenton oxidation processes, *Water Res.* 37 (2003) 1308–1319.
- X. Zhao, A. Li, R. Mao, H. Liu, J. Qu, Electrochemical removal of haloacetic acids in a three-dimensional electrochemical reactor with Pd-GAC particles as fixed filler and Pd-modified carbon paper as cathode, *Water Res.* 51 (2014) 134–143.
- C. Zhang, Y. Jiang, Y. Li, Z. Hu, L. Zhou, M. Zhou, Three-dimensional electrochemical process for wastewater treatment: a general review, *Chem. Eng. J.* 228 (2013) 455–467.
- L. Yan, H. Ma, B. Wang, Y. Wang, Y. Chen, Electrochemical treatment of petroleum refinery wastewater with three-dimensional multi-phase electrode, *Desalination* 276 (2011) 397–402.
- S. Ammar, M.A. Oturan, L. Labiadh, A. Guersalli, R. Abdelhedi, N. Oturan, E. Brillas, Degradation of tyrosol by a novel electro-Fenton process using pyrite as heterogeneous source of iron catalyst, *Water Res.* 74 (2015) 77–87.
- Y. Segura, F. Martínez, J.A. Melero, Effective pharmaceutical wastewater degradation by Fenton oxidation with zero-valent iron, *Appl. Catal. B-Environ.* 136–137 (2013) 64–69.
- T.W. Leal, L.A. Lourenço, H.L. Brandão, A. Silva, S.M.A.G.U. Souza, A.A.U. Souza, Low-cost iron-doped catalyst for phenol degradation by heterogeneous Fenton, *J. Hazard. Mater.* 359 (2018) 93–103.
- F. Duarte, F.J. Maldonado-Hódar, L.M. Madeira, New insight about orange II elimination by characterization of spent activated carbon/Fe Fenton-like catalysts, *Appl. Catal. B-Environ.* 129 (2013) 264–272.
- J. Herney-Ramirez, M.A. Vicente, L.M. Madeirac, Heterogeneous photo-Fenton oxidation with pillared clay-based catalysts for wastewater treatment: a review, *Appl. Catal. B-Environ.* 98 (2010) 10–26.
- Y. Liu, Q. Fan, J.L. Wang, Zn-Fe-CNTs catalytic in situ generation of H_2O_2 for Fenton-like degradation of sulfamethoxazole, *J. Hazard. Mater.* 342 (2018) 166–176.
- B. Sun, Y.Z. Long, H.D. Zhang, M.M. Li, J.L. Duvail, X.Y. Jiang, H.L. Yin, Advances in three-dimensional nanofibrous macrostructures via electrospinning, *Prog. Polym. Sci.* 39 (2014) 862–890.
- B. Bolto, T. Tran, M. Hoang, Z.L. Xie, Crosslinked poly(vinyl alcohol) membranes, *Prog. Polym. Sci.* 34 (2009) 969–981.
- M. Stefaniuk, P. Oleszczuk, Y.S. Ok, Review on nano zerovalent iron (nZVI): from synthesis to environmental applications, *Chem. Eng. J.* 287 (2016) 618–632.
- P. Thavarungkul, P. Kanatharana, An enzyme sensor for urea based on conductivity measurement, *J. Sci. Soc. Thailand* 20 (1994) 23–30.
- X.B. Hu, B.Z. Liu, Y.H. Deng, H.Z. Chen, S. Luo, C. Sun, P. Yang, S.G. Yang, Adsorption and heterogeneous Fenton degradation of 17-methyltestosterone on nano Fe_3O_4 /MWCNTs in aqueous solution, *Appl. Catal. B-Environ.* 107 (2011) 274–283.
- Q. Liu, L. Zhong, Q. Zhao, C. Frear, Y. Zheng, Synthesis of Fe_3O_4 /polyacrylonitrile composite electrospun nanofiber mat for effective adsorption of tetracycline, *ACS Appl. Mater. Inter.* 7 (2015) 14573–14583.
- Y.M. Zheng, L. Yu, D. Wu, J.P. Chen, Removal of arsenite from aqueous solution by

- a zirconia nanoparticle, *Chem. Eng. J.* 188 (2012) 15–22.
- [28] J. Wang, Z.W. Liao, J. Lfthikar, L. Shi, Y.N. Du, J.Y. Zhu, S. Xi, Z.Q. Chen, Z.L. Chen, Treatment of refractory contaminants by sludge-derived biochar/persulfate system via both adsorption and advanced oxidation process, *Chemosphere* 185 (2017) 754–763.
- [29] G.H. Li, Z.G. Zhao, B.Y. Qi, G.J. Liu, P. Wu, G.F. Zeng, Y.F. Zhang, W. Wang, Y.H. Sun, Rapid capture of Ponceau S via a hierarchical organic-inorganic hybrid nanofibrous membrane, *J. Mater. Chem. A Mater. Energy Sustain.* 4 (2016) 5423–5427.
- [30] H. Niu, D. Zhang, S. Zhang, X. Zhang, Z. Meng, Y. Cai, Humic acid coated Fe₃O₄ magnetic nanoparticles as highly efficient Fenton-like catalyst for complete mineralization of sulfathiazole, *J. Hazard. Mater.* 190 (2011) 559–565.
- [31] A. Fabiańska, A. Bialk-Bielińska, P. Stepnowski, S. Stolte, E.M. Siedlecka, Electrochemical degradation of sulfonamides at BDD electrode: kinetics, reaction pathway and eco-toxicity evaluation, *J. Hazard. Mater.* 280 (2014) 579–587.
- [32] A.C. Velosa, C.A.O. Nascimento, Evaluation of sulfathiazole degradation by persulfate in Milli-Q water and in effluent of a sewage treatment plant, *Environ. Sci. Pollut. Res.* 24 (2017) 6270–6277.
- [33] A.P.S. Batista, R.F.P. Nogueira, Parameters affecting sulfonamide photo-Fenton degradation - iron complexation and substituent group, *J. Photochem. Photobiol. A: Chem.* 232 (2012) 8–13.
- [34] A.P.S. Batista, B.A. Cottrell, R.F.P. Nogueira, Photochemical transformation of antibiotics by excitation of Fe(III)-complexes in aqueous medium, *J. Photochem. Photobiol. A: Chem.* 274 (2014) 50–56.
- [35] M. Velásquez, I.P. Santander, D.R. Contreras, J. Yáñez, C. Zaror, R.A. Salazar, M. Pérez-Moya, H.D. Mansilla, Oxidative degradation of sulfathiazole by Fenton and photo-Fenton reactions, *J. Environ. Sci. Heal. A* 49 (2014) 661–670.
- [36] X. Zhang, B. Bai, G.L. Puma, H.L. Wang, Y.R. Suo, Novel sea buckthorn biocarbon SBC@β-FeOOH composites: Efficient removal of doxycycline in aqueous solution in a fixed-bed through synergistic adsorption and heterogeneous Fenton-like reaction, *Chem. Eng. J.* 284 (2016) 698–707.
- [37] X.P. Wei, H.H. Wu, G.P. He, Y.F. Guan, Efficient degradation of phenol using iron-montmorillonite as a Fenton catalyst: importance of visible light irradiation and intermediates, *J. Hazard. Mater.* 321 (2017) 408–416.
- [38] T. Zhou, Y.Z. Li, J. Ji, F. Wong, X.H. Lu, Oxidation of 4-chlorophenol in a heterogeneous zero valent iron/H₂O₂ Fenton-like system: kinetic, pathway and effect factors, *Sep. Purif. Technol.* 62 (2008) 551–558.
- [39] A.M. Wang, Y.Y. Zhang, H.H. Zhong, Y. Chen, X.J. Tian, D.S. Li, J.Y. Li, Efficient mineralization of antibiotic ciprofloxacin in acid aqueous medium by a novel photoelectro-Fenton process using a microwave discharge electrodeless lamp irradiation, *J. Hazard. Mater.* 342 (2018) 364–374.
- [40] N. López, S. Plaza, A. Afkhami, P. Marco, J. Giménez, S. Esplugas, Treatment of Diphenhydramine with different AOPs including photo-Fenton at circumneutral pH, *Chem. Eng. J.* 318 (2017) 112–120.